Article

TRANSPARENT PROCESS

THE EMBO JOURNAL

YAP-TEAD signaling promotes basal cell carcinoma development via a c-JUN/AP1 axis

Dejan Maglic[1,2,†], Karin Schlegelmilch[3], Antonella FM Dost[1], Riccardo Panero[4], Michael T Dill[1,2,§], Raffaele A Calogero[4] & Fernando D Camargo[1,2,*]

Abstract

The mammalian Hippo signaling pathway, through its effectors YAP and TAZ, coerces epithelial progenitor cell expansion for appropriate tissue development or regeneration upon damage. Its ability to drive rapid tissue growth explains why many oncogenic events frequently exploit this pathway to promote cancer phenotypes. Indeed, several tumor types including basal cell carcinoma (BCC) show genetic aberrations in the Hippo (or YAP/TAZ) regulators. Here, we uncover that while YAP is dispensable for homeostatic epidermal regeneration, it is required for BCC development. Our clonal analyses further demonstrate that the few emerging Yap-null dysplasia have lower fitness and thus are diminished as they progress to invasive BCC. Mechanistically, YAP depletion in BCC tumors leads to effective impairment of the JNK-JUN signaling, a well-established tumor-driving cascade. Importantly, in this context, YAP does not influence canonical Wnt or Hedgehog signaling. Overall, we reveal Hippo signaling as an independent promoter of BCC pathogenesis and thereby a viable target for drug-resistant BCC.

Keywords AP1; basal cell carcinoma; Hippo signaling; Jun; YAP
Subject Categories Cancer; Signal Transduction; Transcription
DOI 10.15252/embj.201798642 | Received 14 November 2017 | Revised 13 June 2018 | Accepted 14 June 2018 | Published online 23 July 2018
The EMBO Journal (2018) 37: e98642

See also: **MM Miranda & WE Lowry** (September 2018)

Introduction

Initially discovered in *Drosophila*, the mammalian Hippo signaling pathway is a central modulator of progenitor cell state necessary for proper epithelial tissue regeneration. The culminating effect of the upstream Hippo kinases and/or cytoskeleton-bound adaptor proteins is to tightly regulate the Hippo effectors' (YAP and TAZ) interaction with the DNA-binding TEA domain (TEAD) transcription factors (Patel *et al*, 2017). Coordinated YAP/TAZ-TEAD interaction and resulting gene signature is vital for embryonic tissue development, as any perturbation in their function results in the depletion of progenitor cell pool and failed organogenesis (Varelas, 2014). The robust propensity of activated YAP and TAZ to enhance the progenitor cell state phenotype (i.e., self-renewal, epithelial–mesenchymal transition, proliferation, and survival) in epithelial cells is believed to be the reason why cancer cells frequently hijack the Hippo pathway during tumorigenesis (Harvey *et al*, 2013). Indeed, conditional YAP overexpression results in hyperproliferation and tumor development in several epithelial tissues including skin epidermis. Short-term epidermal YAP overexpression induces the expansion of undifferentiated/progenitor cells in the interfollicular epidermis (IFE), skin thickening, and development of basal cell carcinoma-like (BCC) lesions (Schlegelmilch *et al*, 2011; Silvis *et al*, 2011; Zhang *et al*, 2011; Akladios *et al*, 2017).

Basal cell carcinoma is the most common sporadic tumor type in individuals of European descent, and its incidence has increased at a steady and alarming rate (Flohil *et al*, 2013; Wu *et al*, 2013). Histologically, BCCs closely resemble expanded IFE basal progenitor cells that have invaded into underlying dermis (Youssef *et al*, 2010; Sanchez-Danes *et al*, 2016). Sporadic human BCC is initiated and driven by mutations in the Hedgehog pathway regulators, mainly the receptor Patched 1 (*PTCH1*) and G-protein-coupled receptor Smoothened (*SMO*). Mutation in *PTCH1* or *SMO* relieves PTCH1 inhibitory effect on SMO and triggers constitutive activation of the GLI-driven growth-promoting programs (Johnson *et al*, 1996; Reifenberger *et al*, 2005; Epstein, 2008). Strong genetic evidence and near 100% mutation frequency of the Hedgehog pathway in basal cell nevus syndrome and BCC have led to successful development of the SMO inhibitor, vismodegib, for the treatment of these diseases. However, locally advanced and metastatic BCCs frequently (~50% recurrence) escape Hedgehog pathway inhibition, predominantly via the mutation of *SMO* within the drug-binding pocket or the alternative potentiation of GLI signaling (Atwood *et al*, 2012, 2015; Sharpe *et al*, 2015; Zhao *et al*, 2015; Danhof *et al*, 2018). The development of new approaches to inhibit BCC tumor growth in parallel with vismodegib therapy would provide significant clinical benefits for patients with advanced BCC.

1 Stem Cell Program, Boston Children's Hospital, Boston, MA, USA
2 Department of Stem Cell and Regenerative Biology, Harvard University, Cambridge, MA, USA
3 The Francis Crick Institute, Tumour Cell Biology, London, UK
4 Molecular Biotechnology Center, Department of Molecular Biotechnology and Health Sciences, University of Torino, Turin, Italy
*Corresponding author. Tel: +1 617 919 2102; E-mail: fernando.camargo@childrens.harvard.edu
†Present address: Relay Therapeutics, Cambridge, MA, USA
§Correction added online on 3 September after first online publication: the author's middle initial has been added.

Phenotypic overlap in the skin with perturbed Hedgehog or Hippo signaling implies that these two pathways might cooperate in the transformation process (Nieuwenhuis *et al*, 2007; Villani *et al*, 2010; Schlegelmilch *et al*, 2011; Zhang *et al*, 2011). Indeed, *YAP* gene amplification and overexpression were found in Hedgehog-driven medulloblastoma (Fernandez *et al*, 2009). The latest genomic analyses of human BCC samples revealed that up to 30% patients' tumors harbor loss-of-function alterations in the known Hippo regulators (Bonilla *et al*, 2016). Hence, in this report we set out to investigate the functional relevance of Hippo pathway output in Hedgehog-driven BCC development. Our rigorous *in vitro* and *in vivo* analyses demonstrate that YAP, but not TAZ, is required for BCC initiation and progression to advanced stage. Functionally, YAP potentiated the well-established JNK-JUN signaling network to drive BCC growth, without any impact on Wnt or Hedgehog signaling. Our data indicate that targeting the Hippo/YAP pathway could offer a novel therapeutic avenue for BCC patients with advanced disease.

Results

YAP is dispensable for normal epidermal homeostasis but upregulated in BCC

Previous studies from our laboratory and others have demonstrated the importance of the Hippo effector, YAP, in epidermal development during embryogenesis (Schlegelmilch *et al*, 2011; Silvis *et al*, 2011; Zhang *et al*, 2011). We sought to investigate YAP function in adult epidermis by conditional *Yap* deletion in 8-week-old mice. Compared to embryonic *Yap* knockout, the adult epidermis showed no evidence of macroscopic or histologic abnormalities in *Yap*-null epidermis during unperturbed homeostatic tissue maintenance up to 12 weeks following *Yap* knockout (Fig EV1A). However, conditions such as wound healing, which require rapid basal progenitor cell expansion to regenerate damaged epidermis, critically depend on YAP function (Lee *et al*, 2014; Elbediwy *et al*, 2016). Thus, we explored the possibility that the Hippo effector, YAP, may be involved in BCC development, a process with uncontrolled expansion of basal progenitor cells (Youssef *et al*, 2010, 2012; Sanchez-Danes *et al*, 2016). First, we assessed YAP expression pattern in 26 human BCC samples by immunohistochemistry (IHC). In 24 out of 26 BCC samples (~92%) analyzed, YAP was highly expressed and localized to the nucleus in the basally located epithelial tumor cells (i.e., tumor cells adjacent to surrounding dermis/mesenchyme) (Fig 1A). Next, we studied YAP expression in a mouse model of BCC ($R26^{LSL\text{-}SmoM2YFP/+}$:*K14CreER*), which develops invasive tumors in ear and tail epidermis 10 weeks postexpression of mutant Smoothened (Youssef *et al*, 2010). Similarly to human BCC, mouse tumors showed robust nuclear YAP localization in the basal tumor cells (Fig 1B). Using *in situ* hybridization, we further compared Yap and Taz mRNA expression patterns in mouse BCC. Whereas Yap mRNA was highly expressed in epithelial BCC cells with particular enrichment in the basal compartment of dermis invading tumor clones, Taz mRNA was predominately expressed in the surrounding mesenchyme (Figs 1C and EV1B). Thus, we speculated that YAP, but not TAZ, is more likely the Hippo effector contributing to the BCC epithelial cell phenotype. Although YAP nuclear versus cytoplasmic localization has been widely used as a measure of Hippo transcriptional output (i.e., Hippo kinases/adaptor proteins inactivity), we sought to better define *in situ* YAP activity within BCC tumors. We crossed transgenic mice with a *Cyr61* BAC promoter driving eGFP expression ($Cyr61^{eGFP}$), a well-established and canonical YAP target gene, with the $R26^{LSL\text{-}SmoM2YFP/+}$:*K14CreER* BCC model (Heintz, 2004; Galli *et al*, 2015; Stein *et al*, 2015; Zanconato *et al*, 2015). Although most normal basal keratinocytes show robust nuclear YAP localization, the eGFP ($Cyr61^{eGFP}$) marks rare basal keratinocytes and mostly cells within sebaceous gland (Figs 1D and EV1A). In BCC tumors, we observed a robust increase in the mosaic eGFP signal in $Cyr61^{eGFP}$:$R26^{SmoM2YFP}$ compared to background uniform YFP expression in $R26^{SmoM2YFP}$ (SmoM2-YFP expression) alone (Figs 1D and EV1C). In other words, we could differentiate a subset of cells with transcriptionally active YAP (i.e., activated $Cyr61^{eGFP}$) within a tumor clone where each BCC cell uniformly expresses SmoM2-YFP (Fig EV1C). In agreement with YAP localization observed by IHC, IF, and RNAscope (Figs 1B and D, and EV1B and C), a strong punctate eGFP signal in $Cyr61^{eGFP}$:$R26^{SmoM2YFP}$ was preferentially found in basally located BCC cells. Overall, we demonstrate the dispensable nature of the Hippo effector, YAP, in adult epidermal homeostasis and specific upregulation of YAP nuclear localization and activity in both human and mouse BCC.

BCC development and tumor progression critically depend on YAP-TEAD interaction

In order to investigate YAP's contribution during BCC development, we crossed the $R26^{LSL\text{-}SmoM2YFP/+}$:*K14CreER* mice onto either $Yap^{+/+}$ or $Yap^{fl/fl}$ backgrounds. The BCC tumors were induced using high-dose tamoxifen starting at postnatal days P24–28 and monitored for visible tumor onset in ear and tail skin (Fig 2A). Whereas $Yap^{+/+}$ mice developed macroscopic BCC in the ear epidermis starting at 8 weeks after tamoxifen administration, *Yap* loss ($Yap^{fl/fl}$ background) significantly rescued visible tumor burden (Fig 2B). In fact, $Yap^{+/+}$ mice required euthanasia on average 12 weeks after tamoxifen administration due to necrotic ear epidermis, while $Yap^{fl/fl}$ succumbed to BCC after ~21.7 weeks ($\chi^2 = 29.95$; $P < 0.0001$, Fig 2B and C). The apparent reduction in tumor burden in $Yap^{fl/fl}$ versus $Yap^{+/+}$ mice was also observed at a histologic level when compared at the stage where dysplastic clones appear (4 weeks after tamoxifen) as well as later (10 weeks after tamoxifen), at which point BCCs have invaded the underlying dermis (Figs 2D and EV2A). Importantly, all the $Yap^{fl/fl}$ mice eventually developed invasive BCC tumors that were Cre-driven recombination escapers for *Yap* bi-allelic knockout (i.e., YAP-positive by IHC), further supporting YAP's critical function in BCC development and progression (Figs 2B and C, and EV2B). We further validated specificity of the $Cyr61^{eGFP}$ reporter for YAP activity in BCC by assessing eGFP expression in *Yap*-null tumor clones ($Yap^{fl/fl}$:$R26^{SmoM2YFP/+}$:*K14CreER*:$Cyr61^{eGFP}$). Indeed, YAP-negative tumor clones or individual cells show baseline YFP/eGFP expression (i.e., equivalent to SmoM2-YFP alone) compared to robust YFP/eGFP expression in a subset of YAP-positive BCCs (Appendix Fig S1A).

While Yap RNAi alone inhibited the proliferation of two mouse BCC cell lines (ASZ and BSZ), combined Yap/Taz RNAi provided additive growth suppression *in vitro* (Fig EV2C; So *et al*, 2006). Although Taz mRNA detection in the mesenchyme surrounding BCC suggested unlikely contribution to epithelial tumor growth, our

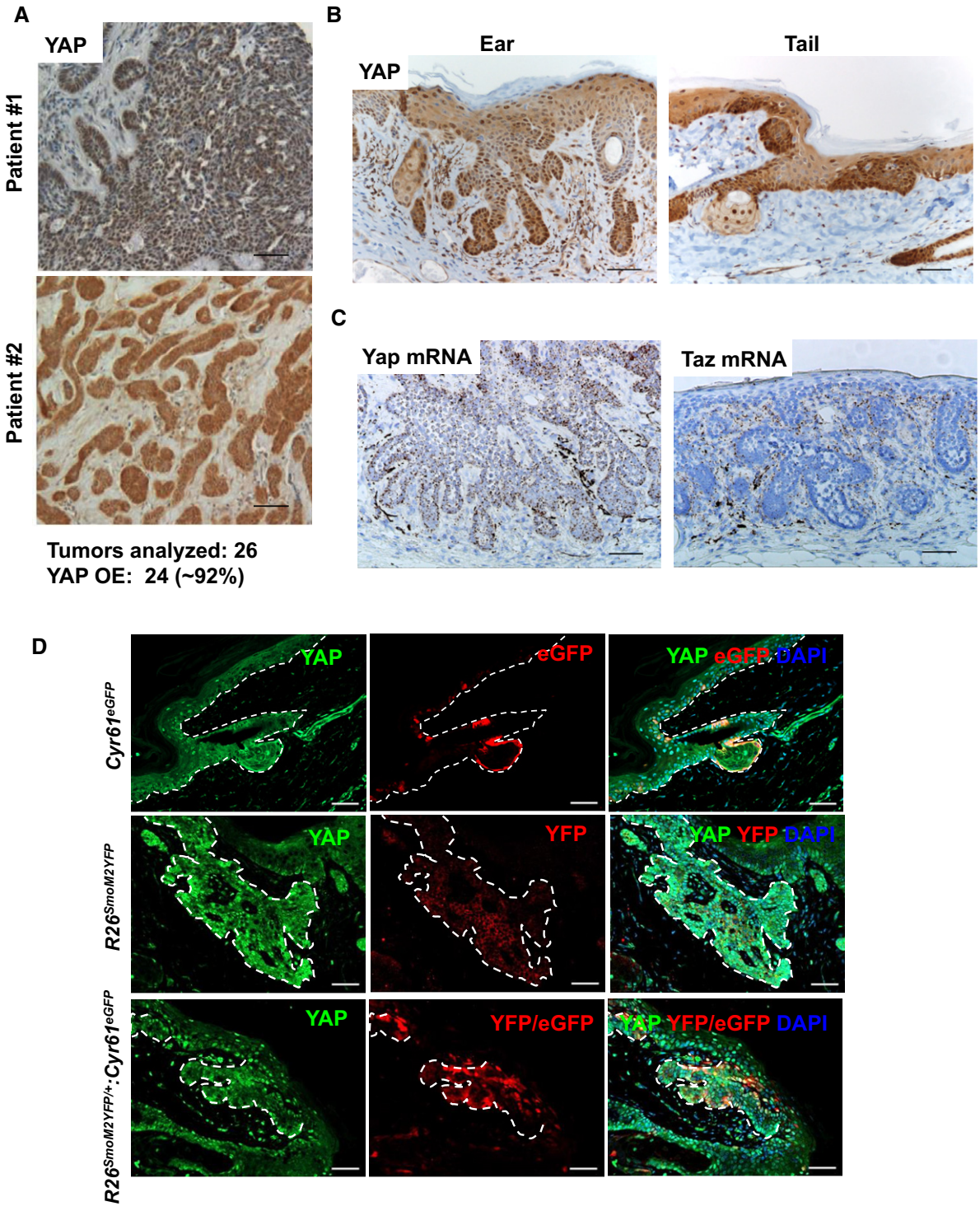

Figure 1. YAP is highly express and localized to nucleus in human and mouse BCC.

A Representative YAP IHC images from analyses of human BCC samples. 24 out of 26 (~92%) BCC cases analyzed showed YAP overexpression (YAP OE) and nuclear localization. Scale bar is 50 μm.

B YAP IHC in ear and tail BCC tumors from the $R26^{LSL\text{-}SmoM2YFP/+}$:*K14CreER* (mutant *Smo*) mouse model. Scale bar is 50 μm.

C RNAscope detection of Yap and Taz mRNA in mouse ear BCC. Scale bar is 50 μm.

D YAP activity in BCC tumors assessed using $Cyr61^{eGFP}$ transgenic reporter mouse. $Cyr61^{eGFP}$ transgenic mouse (upper panels) was crossed with $R26^{LSL\text{-}SmoM2YFP/+}$:*K14CreER* ($R26^{SmoM2YFP/+}$:$Cyr61^{eGFP}$; bottom panels) and compared with $R26^{LSL\text{-}SmoM2YFP/+}$:*K14CreER* ($R26^{SmoM2YFP/+}$; middle panels). YFP denotes SmoM2-YFP fusion gene expression. eGFP denotes $Cyr61^{eGFP}$ expression. Upper panels: Dashed lines mark separation between basal epidermal cells and dermis. Middle and lower panels: Dashed lines outline BCC clones. Scale bar is 50 μm.

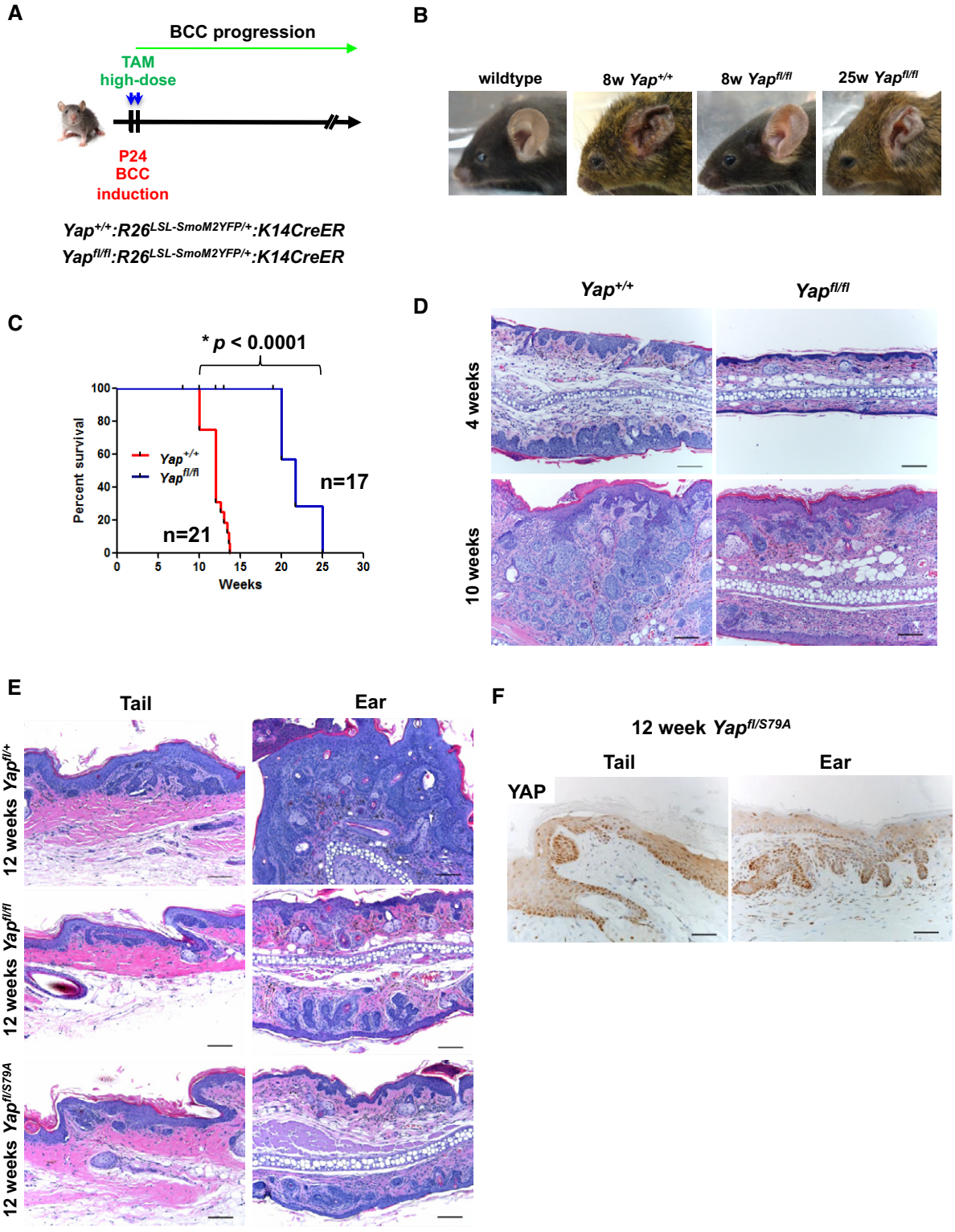

Figure 2. *Yap* deletion significantly reduces tumor burden in BCC mouse model.

A Scheme representing the genetic strategy used to induce BCC in mouse epidermis.

B Representative images of macroscopic tumor burden in mouse ears from $Yap^{+/+}$ and $Yap^{fl/fl}$ at 8 and 25 weeks after tamoxifen.

C Kaplan–Meier survival curve comparing $Yap^{+/+}$ with $Yap^{fl/fl}$ mice. The groups were compared using log-rank (Mantel–Cox) test. *$P < 0.0001$.

D Representative histological analysis of ear BCC from $Yap^{+/+}$ and $Yap^{fl/fl}$. Scale bar is 100 μm.

E BCC histology comparing $Yap^{fl/+}$, $Yap^{fl/fl}$, and $Yap^{fl/S79A}$ mutant backgrounds (YAP^{S79A} does not bind TEAD transcription factors). Scale bar is 100 μm.

F YAP IHC in $Yap^{fl/S79A}$ background demonstrating YAP expression and nuclear localization. Scale bar is 50 μm.

in vitro data suggested that Taz might provide a compensatory mechanism in the *Yap*-null BCC clones. To address TAZ contribution in BCC, we first validated YAP-specific and YAP/TAZ antibodies using epidermis from *TetO-Cre rtTA* $Yap^{fl/fl}$ mice to show a low but detectable signal with YAP/TAZ antibody (i.e., TAZ protein) in *Yap*-null ear and tail basal keratinocytes (Appendix Fig S2A). Next, we performed IHC in the $Yap^{fl/fl}$ BCC serial sections with YAP and YAP/TAZ antibodies to demonstrate extremely low or undetectable TAZ signal with YAP/TAZ antibody in the *Yap*-null BCC (Appendix Fig S2B). We confirmed a decrease in Taz mRNA expression in the *Yap*-null BCC using FACS-sorted tumors (Appendix Fig S2C). Finally, we crossed the $R26^{LSL\text{-}SmoM2YFP/+}$:*K14CreER* mice onto the $Yap^{fl/fl}$ and $Taz^{fl/fl}$ backgrounds to genetically assess TAZ contribution in BCC tumor initiation and progression. When compared at 8 weeks after tamoxifen administration, *Yap/Taz* or *Yap* knockout-alone BCCs were indistinguishable upon histologic and tumor clone size analyses (Appendix Fig S2D–E). Hence, our data strongly support that YAP specifically drives BCC growth without significant compensation from TAZ in the *Yap*-null tumors.

Since the majority of known YAP growth-promoting properties have been attributed to its interaction with the DNA-binding transcription factors, TEAD, we investigated the necessity of YAP-TEAD interaction in BCC. We took advantage of the already established Yap^{S79A} allele, a mutant YAP that does not bind TEAD, and crossed it onto the BCC model to establish $Yap^{fl/S79A}$:$R26^{LSL\text{-}SmoM2YFP/+}$:*K14CreER* (Schlegelmilch *et al*, 2011). Thus, upon tamoxifen induction, the wild-type *Yap* allele was floxed out, allowing only expression of the Yap^{S79A} in BCC tumors, which closely phenocopied $Yap^{fl/fl}$ when compared to $Yap^{+/+}$ BCC tumors (Fig 2E and F). Notably, no phenotypic differences were detected between $Yap^{fl/+}$ and $Yap^{+/+}$ backgrounds, indicating that YAP is not haplo-insufficient for BCC development (data not shown). Therefore, our data strongly support the notion that YAP promotes BCC growth by direct interaction with TEAD transcription factors.

To more precisely evaluate the relative behavior of BCC clones, tumors in the $Yap^{fl/fl}$:$R26^{LSL\text{-}SmoM2YFP/+}$:*K14CreER* background were induced with low-dose tamoxifen (Fig 3A). The longitudinal tracking of the *Yap*-null versus *Yap*-positive clonal evolution began 4 weeks after tamoxifen induction, when dysplastic tumors appear, and was continued until 20 weeks, when most clones have already acquired the invasive phenotype (Fig 3B; Youssef *et al*, 2012; Sanchez-Danes *et al*, 2016). Overall, we observed a significant and time-dependent reduction in the percentage of *Yap*-null BCC clones in ear and tail epidermis (Fig 3C). Our analysis of absolute *Yap*-null clone numbers at each time point indicates that they are not only outcompeted by the *Yap*-positive tumor cells, but also specifically depleted over time (Fig 3D). In other words, although we could detect a significant number of established dysplastic *Yap*-null BCC clones at 4 weeks, their number was diminished as the tumors progressed to invasive BCC (10- to 20-week time points). Lastly, we analyzed relative BCC clone size between $Yap^{+/+}$, $Yap^{fl/fl}$, and $Yap^{fl/S79A}$ backgrounds at the 12-week time point. By further differentiating *Yap*-null versus *Yap*-positive BCC clones in the $Yap^{fl/fl}$ background using IHC, we demonstrate that YAP, and its interaction with TEAD, is critical for BCC clone expansion (*Yap*-null vs. *Yap*-positive; *Yap*-null vs. $Yap^{+/+}$; and $Yap^{+/+}$ vs. $Yap^{fl/S79A}$; $P < 0.05$; Fig 3E). Hence, our data reveal that YAP loss or disruption in YAP-TEAD interaction significantly impairs BCC establishment and tumor progression from dysplasia to an invasive phenotype.

YAP transcriptional gene signature drives BCC cell proliferation independent of Wnt or Hedgehog signaling

Following the observation that *Yap* loss leads to a strong growth-deficit phenotype in BCC, we set out to understand the mechanistic nature by which YAP drives tumor growth**.** Using EdU pulse-chase *in vivo*, we show that *Yap*-null clones have impaired proliferation compared to their neighboring *Yap*-positive tumor clones (Fig 4A and B). This observation is in line with the observed decrease in proliferation upon Yap knockdown in two BCC cell lines (Fig EV2C). The activity of the most commonly mutated pathway in BCC, Hedgehog, and its cooperation with Wnt signaling are considered to be absolutely necessary for BCC growth and survival (Yang *et al*, 2008; Atwood *et al*, 2012; Youssef *et al*, 2012). Hence, we foremost studied whether *Yap* loss has an impact on Wnt or Hedgehog signaling outputs and thereby impairs BCC growth. Using serial sections from the $Yap^{fl/fl}$ BCC tumor, we show no change in β-catenin nuclear localization between YAP-negative and YAP-positive clones (Fig 4C). Wnt activity in BCC establishes an embryonic hair follicle (EHF) phenotype that is marked by an expression of PCDH, LEF1, CUX1, and LHX2, none of which were found affected in the *Yap*-null BCC clones (Fig EV3A; Ito *et al*, 2007; Youssef *et al*, 2012). The canonical Wnt target genes, Axin2 and Lgr5, and a well-established BCC stemness-promoting transcription factor, SOX9, were also unaffected in YAP-negative BCC (Fig EV3B; Youssef *et al*, 2012; Larsimont *et al*, 2015). Equally, *Yap* loss had no impact on the canonical Hedgehog target genes in BCC, Gli1 or Ptch1 (Fig 4D). Therefore, our data support the notion that YAP promotes BCC growth independent of Wnt and Hedgehog signaling.

In order to identify the YAP-driven gene signature that contributes to the BCC phenotype, we performed RNAseq ($Yap^{+/+}$ vs. $Yap^{fl/fl}$) and ChIPseq (TEAD1, TEAD4, and H3K27Ac) analyses in the established BCC. First, we confirmed that combining tdTomato reporter with SmoM2-YFP ($R26^{LSL\text{-}SmoM2YFP/LSL\text{-}tdTom}$) allows us to purify BCC cells at 6 weeks after high-dose tamoxifen, a time point when we observe the highest *Yap* knockout efficiency (~70%) in the ear BCCs (Appendix Fig S3A–C). Hence, the RNAseq was performed on the FACS-sorted (DAPI/CD45/TER119 negative, tdTomato/α6-integrin positive) $Yap^{+/+}$ and $Yap^{fl/fl}$ ear BCC cells 6 weeks after high-dose tamoxifen administration (Fig 5A). Differential gene expression analysis identified 97 genes that were significantly changed in the *Yap*-null BCC, one of which is the YAP's canonical target gene, Cyr61 (Fig 5B, Table EV1). Of the 97 differentially expressed genes, 57 were bound by TEAD1 and TEAD4 within their TSS or enhancer region (Fig 5C, Table EV2). Thus, our RNAseq and ChIPseq data further support that a YAP-TEAD-driven gene signature directly contributes to BCC growth. Next, we performed Ingenuity Pathway Analysis—IPA (Qiagen), which ranked signaling pathways that are significantly affected by *Yap* loss. Interestingly, the JNK pathway, previously implicated in BCC, showed strongest changes upon *Yap* loss ($P = 2.04 \times 10^{-7}$, Fig 5D; Schnidar *et al*, 2009; Eberl *et al*, 2012). JNK (c-Jun N-terminal kinase) is the upstream kinase that phosphorylates and directly regulates transactivational activity of c-JUN, a member of the AP1 transcriptional complex (Lopez-Bergami *et al*, 2010). Our TEAD1, TEAD4, and

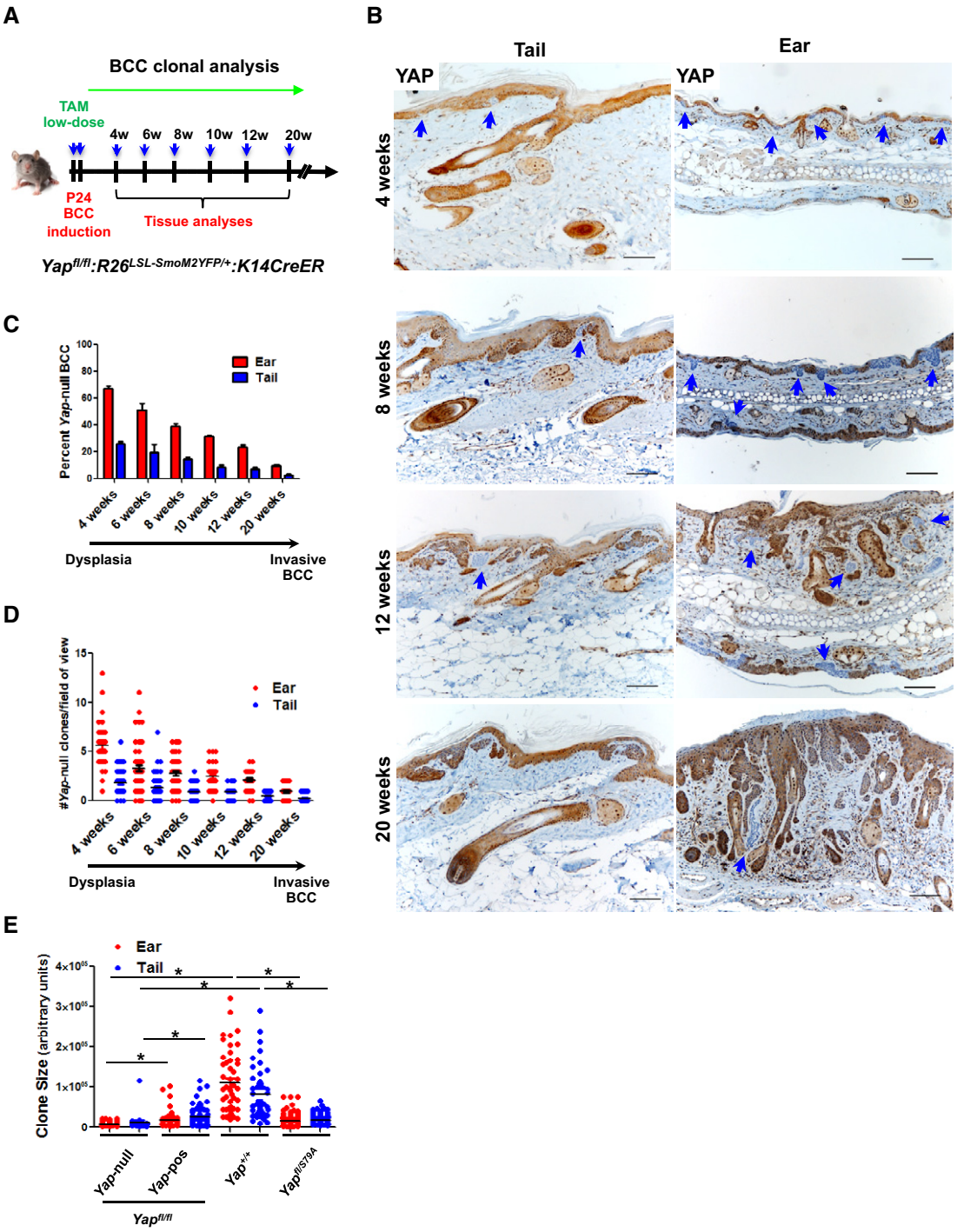

Figure 3. Clonal evolution of *Yap*-null BCC tumors.

A Schematic depiction of clonal *Yap*-null versus *Yap*-positive BCC tracing over time.

B YAP IHC and histological analyses of ear and tail BCC tumors in $Yap^{fl/fl}$ background at indicated time points. Blue arrows indicate *Yap*-null BCC clones. Scale bar is 100 μm.

C Quantification of YAP-positive versus YAP-negative clones at 4, 6, 8, 10, 12, and 20 weeks after low-dose tamoxifen administration. At least three mice per group were analyzed. Error bars indicate SEM.

D Quantification of total number of *Yap*-null clones per field of view in ear and tail skin. Total of three mice per time point were used, and at least eight random fields per mouse were counted for each tissue section. Error bars indicate SEM.

E Ear and tail BCC clone size quantification using ImageJ at 12 weeks after low-dose tamoxifen administration. In $Yap^{fl/fl}$ background, YAP IHC analysis was used to determine *Yap*-positive versus *Yap*-null clones. Total of three mice per genotype were used and at least seven clones were counted per tissue section. The groups were compared using Student's *t*-test. $*P < 0.05$.

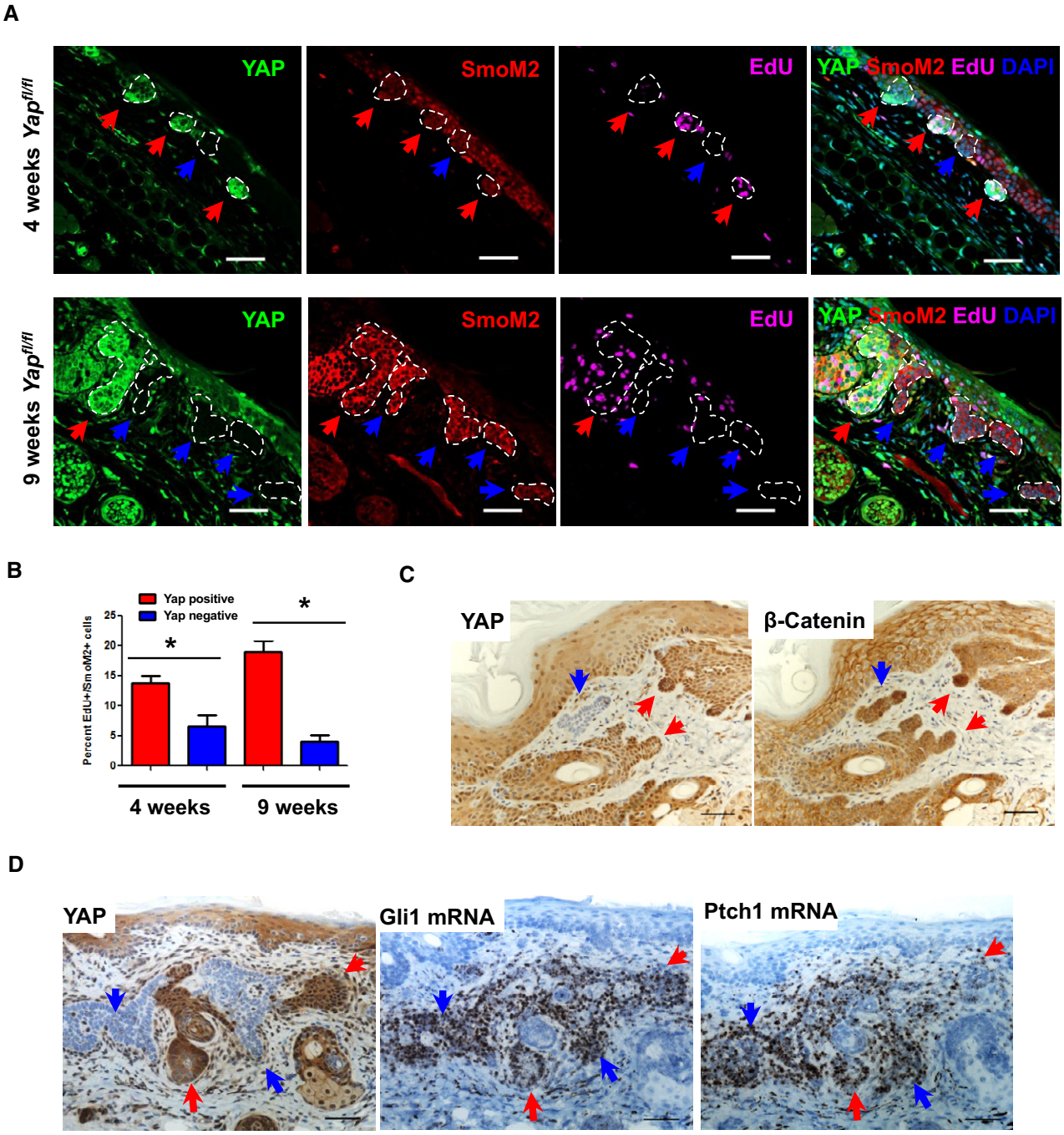

Figure 4. YAP provides proliferative advantage to BCC tumors independent of Wnt or Hedgehog signaling.

A Immunofluorescent imaging of EdU incorporation in the YAP-negative versus YAP-positive clones in *Yap*$^{fl/fl}$ ear BCC. Red arrows indicate YAP-positive clones; blue arrows indicate YAP-negative clones. Scale bar is 50 μm.

B Quantified EdU incorporation in YAP-negative versus YAP-positive dysplastic clones (4 and 9 weeks after tamoxifen). Total of three mice were used per time point, and at least 20 clones per tissue section were quantified. Error bars indicate SEM. The groups were compared using Student's *t*-test *$P < 0.05$.

C YAP and β-catenin IHC in *Yap*$^{fl/fl}$ BCC serial sections. Red arrows indicate YAP-positive clones; blue arrows indicate YAP-negative clones. Scale bar is 50 μm.

D YAP IHC and Gli1/Ptch1 RNAscope in *Yap*$^{fl/fl}$ BCC serial sections. Blue arrows indicate YAP-negative BCC clones; red arrows indicate YAP-positive BCC clones. Scale bar is 50 μm.

H3K27Ac ChIPseq analyses reveal that TEAD strongly binds to known AP1-regulated genes including *c-Jun* (Fig 5E, Table EV3). In fact, Homer *de novo* motif analysis using TEAD1 and TEAD4 ChIPseq peaks confirms the previously described enrichment of the *AP1* consensus motifs within TEAD1 and TEAD4 peaks (Fig EV4A; Zanconato *et al*, 2015; Liu *et al*, 2016). Therefore, our findings

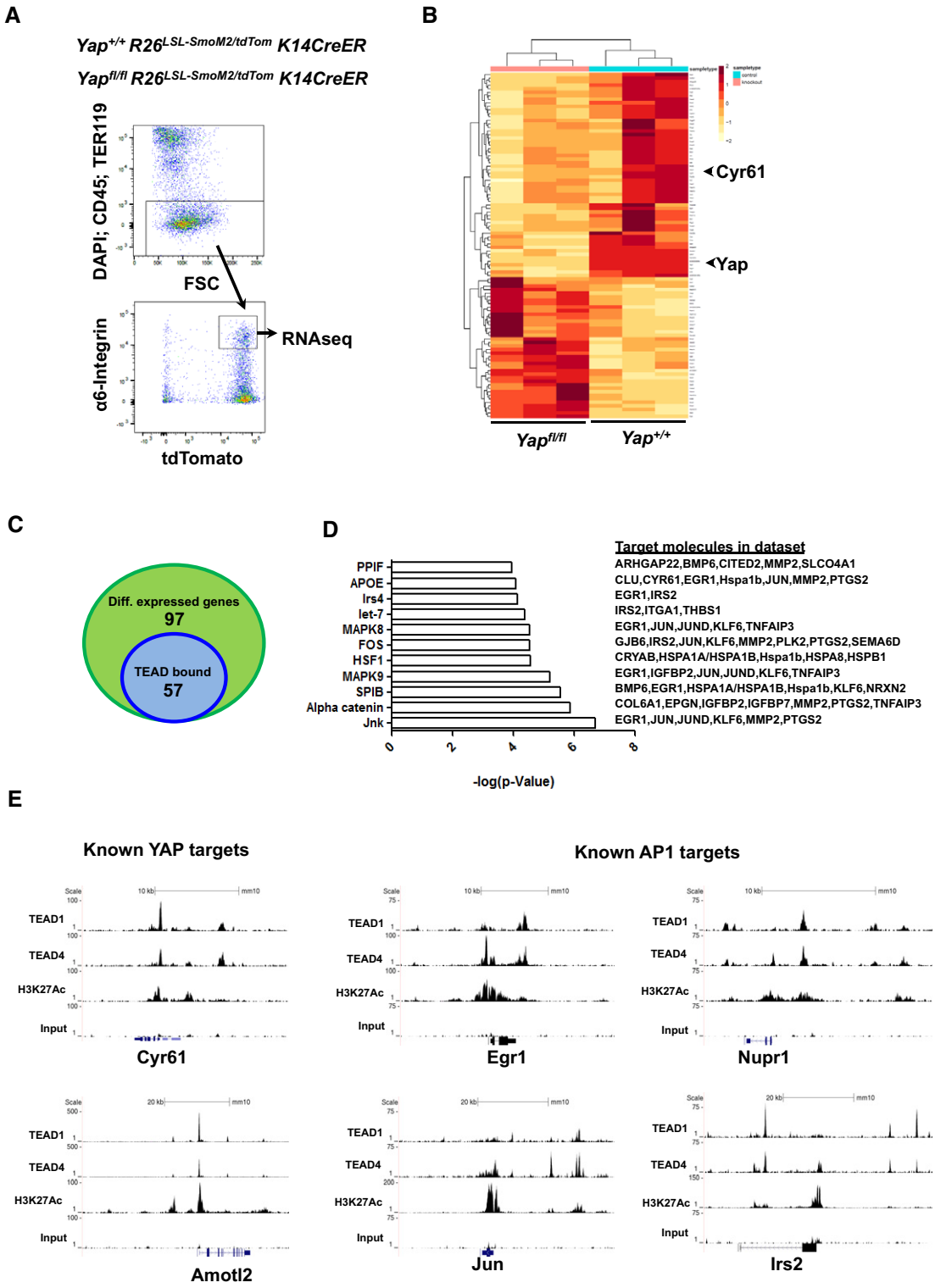

Figure 5. Identification of YAP-driven gene signature in BCC tumors.

A FACS methodology to purify ear BCC cells from *Yap*$^{+/+}$ and *Yap*$^{fl/fl}$ mice (6 weeks after high-dose tamoxifen administration) for RNAseq analysis.

B RNAseq heatmap of differentially expressed genes between *Yap*$^{+/+}$ and *Yap*$^{fl/fl}$ BCC.

C Venn diagram of TEAD1/TEAD4 peaks found within differentially expressed genes from *Yap*-null BCC.

D Ingenuity Pathway Analysis of differentially expressed genes between *Yap*$^{+/+}$ and *Yap*$^{fl/fl}$ BCC.

E TEAD1, TEAD4, H3K27Ac, and input (control) peaks associated with known YAP targets (Cyr61 and AmotL2) or known AP1 targets (Egr1, Jun, Nupr1, Irs2) from BCC ChIPseq.

strongly suggest that YAP cooperates with c-JUN and AP1 activity to induce the gene signature required for BCC initiation and progression.

YAP potentiates JUN stability and activity in BCC to promote tumor growth

Since RNAseq analysis of the *Yap*-null BCC suggested that YAP regulates known AP1 target genes and because we observed TEAD occupancy at those genes, including *c-Jun*, we further assessed how YAP impacts c-JUN activity. First, we validated RNAseq data by qPCR analyses of known YAP (Cyr61, AmotL2, Arhgap29) and AP1 (c-Jun, Fos, Junb, Clu, Egr1, Irs2, Nupr1, Dusp5, Ptgs2, and Igfbp7) target genes, which were significantly downregulated in *Yap*-null BCC (Fig. 6A; Jin & Howe, 1997; Goruppi *et al*, 2002; Troen *et al*, 2004; Cui *et al*, 2006; Hoffmann *et al*, 2008; Okamura *et al*, 2012; Mina *et al*, 2015). Likewise, *in vitro Yap* knockout in ASZ cells with doxycycline (Dox)-inducible Yap sgRNA (TetON-CRISPR-YapKO) recapitulated reduction in AP1 (c-JUN) regulated target genes (Fig EV5A). By taking advantage of transcriptomic cancer cell line data from the Broad-Novartis Cancer Cell Line Encyclopedia (CCLE), we discovered strong c-JUN and FOS mRNA correlation with an activated YAP signature (i.e., CYR61, AMOTL2, ARHGAP29, YAP) across various cancer types (Fig EV4B and C). To determine whether YAP directly affects c-JUN activity, we studied c-JUN expression and activating phosphorylation at two positions (Serine 63 and 73) in YAP-negative and YAP-positive BCCs (Lopez-Bergami *et al*, 2010). Both of the c-JUN phosphorylation sites and total c-JUN were significantly reduced in the YAP-negative BCC (Fig 6B). Next, we studied the status of c-JUN phosphorylation in the BCC clones from $Yap^{fl/fl}$ mice. When compared with YAP-positive clones, YAP-negative BCC clones had significantly decreased c-JUN phosphorylation on serines 63 and 73, the two well-known JNK phosphorylation sites (Fig 6C). In agreement, phosphorylated JNK1/2 (pJNK1/2) was decreased in the same YAP-negative clones relative to the neighboring YAP-positive tumors. The YAP effect on the JNK-JUN pathway activity was recapitulated in the TetON-CRISPR-YapKO ASZ and BSZ cell lines; YAP loss decreased phosphorylation levels of JNK and JUN (Fig 6D). Since the total c-JUN protein, c-JUN phosphorylation, and c-Jun mRNA are simultaneously decreased in the YAP-negative *in vitro* and *in vivo* BCC models, our data suggest that combination of impaired protein stability and gene expression contributes to reduced total c-JUN protein (Figs 6A–D and EV5A). Notably, activated c-JUN protein binds to its own promoter to increase c-Jun mRNA expression, which further contributes to diminished total c-JUN protein in the *Yap*-null BCC (Angel *et al*, 1988).

To further validate YAP as a potential target in BCC and its effect on the JNK-JUN signaling, we established subcutaneous allograft BCC tumors with TetON-CRISPR-YapKO ASZ cells in immunocompromised (*nu/nu*) mice. The injected TetON-CRISPR-YapKO ASZ cells were allowed to establish tumors before mice were randomized to either a control or Dox receiving group. Six weeks following randomization, control mice required euthanasia due to large tumor size; however, mice receiving Dox (induced *Yap* knockout) had significantly reduced tumor burden (Fig EV5B and C). When we analyzed *Yap* knockout efficiency in the mice receiving Dox for 6 weeks, we could detect only a small fraction of *Yap*-null BCC cells relative to the tumors from mice receiving Dox for 1 week (Fig EV5D). This observation suggests that *Yap*-null cells were specifically depleted over time while the cells escaping *Yap* bi-allelic deletion outgrew and repopulated the tumor. Subsequently, we assessed JNK-JUN pathway activity in tumor serial sections from the 1-week Dox-treated or control mice. The *Yap*-null tumors exhibited significant reductions in pJNK1/2, pJUN S63, and pJUN S73 levels relative to the control tumors, further corroborating the link between YAP and JNK-JUN activity (Fig EV5E). To assess sensitivity of BCC cell lines (ASZ and BSZ) to the JNK-JUN pathway inhibition, we analyzed *in vitro* cell proliferation upon treatment with SP600125 (JNK1/2/3 inhibitor). Both of the BCC cell lines were completely impaired in their ability to grow upon SP600125 treatment, which was concomitant with decreased c-JUN phosphorylation (Fig EV6A and B).

Since YAP overexpression is a potent inducer of IFE hyperproliferation, we set to examine the JNK-JUN pathway activation in the YAP-driven lesions. Indeed, doxycycline-inducible YAP^{S127A} (constitutively active) overexpression (*Col1*$^{TetO\text{-}YAPS127A}$ *R26*$^{LSL\text{-}rtTA/+}$ *K14Cre*) in adult epidermis led to ear IFE thickening, which closely resembles BCC tumors. Our analyses demonstrate robust c-JUN (S63 and S73), and weaker JNK1/2 phosphorylation increases in YAP-driven lesions compared to the wild-type ear epidermis (Fig EV6C). Conversely, both c-JUN and JNK1/2 phosphorylation were almost undetectable in the *Yap*-null ear epidermis ($Yap^{fl/fl}$ *TetO-Cre rtTA*) when compared to the wild-type control (Fig EV6C). Hence, our data provide genetic evidence that YAP regulates JNK-JUN activity *in vivo*.

By using human tumor samples, genetically engineered mouse models, and *in vitro* cell lines, our study provides substantial evidence that: (i) YAP is dispensable for homeostatic epidermal regeneration; (ii) YAP activity is enriched in the basal tumor cells of BCC; (iii) YAP-TEAD interaction is required for BCC initiation and tumor maintenance; and (iv) YAP potentiates c-JUN activity to drive BCC growth.

Discussion

Basal cell carcinoma (BCC) is a skin tumor initiated and driven by activating mutations in the Hedgehog signaling pathway (Reifenberger *et al*, 2005; Epstein, 2008). Although the vast majority of BCC are curable with resection, vismodegib (SMO inhibitor) therapy, or a combination of both, the projected increase in BCC incidence over coming decades will result in a surge of advanced and vismodegib-resistant cases (Danhof *et al*, 2018). Additionally, emerging findings suggest that advanced BCC could transdifferentiate into squamous cell carcinoma (SCC) with a much more aggressive phenotype (Orouji *et al*, 2014; Ransohoff *et al*, 2015; Zhao *et al*, 2015). Therefore, identification and validation of novel therapeutic strategies for patients with advanced BCC will be instrumental in preventing cancer-associated death from this disease.

Recent detailed genomic analysis of human BCC tumors has identified alterations in additional pathways, which could contribute to initial tumor growth, invasion, and metastasis, or vismodegib resistance. One of the pathways identified with significant mutational propensity in its regulatory components was the Hippo, whose effectors, YAP and TAZ, have been shown to promote cancer phenotypes in a variety of tissues (Bonilla *et al*, 2016). Genetic alterations within the Hippo regulators have been generally low in other cancers, which elevates the significance of YAP activity in BCC

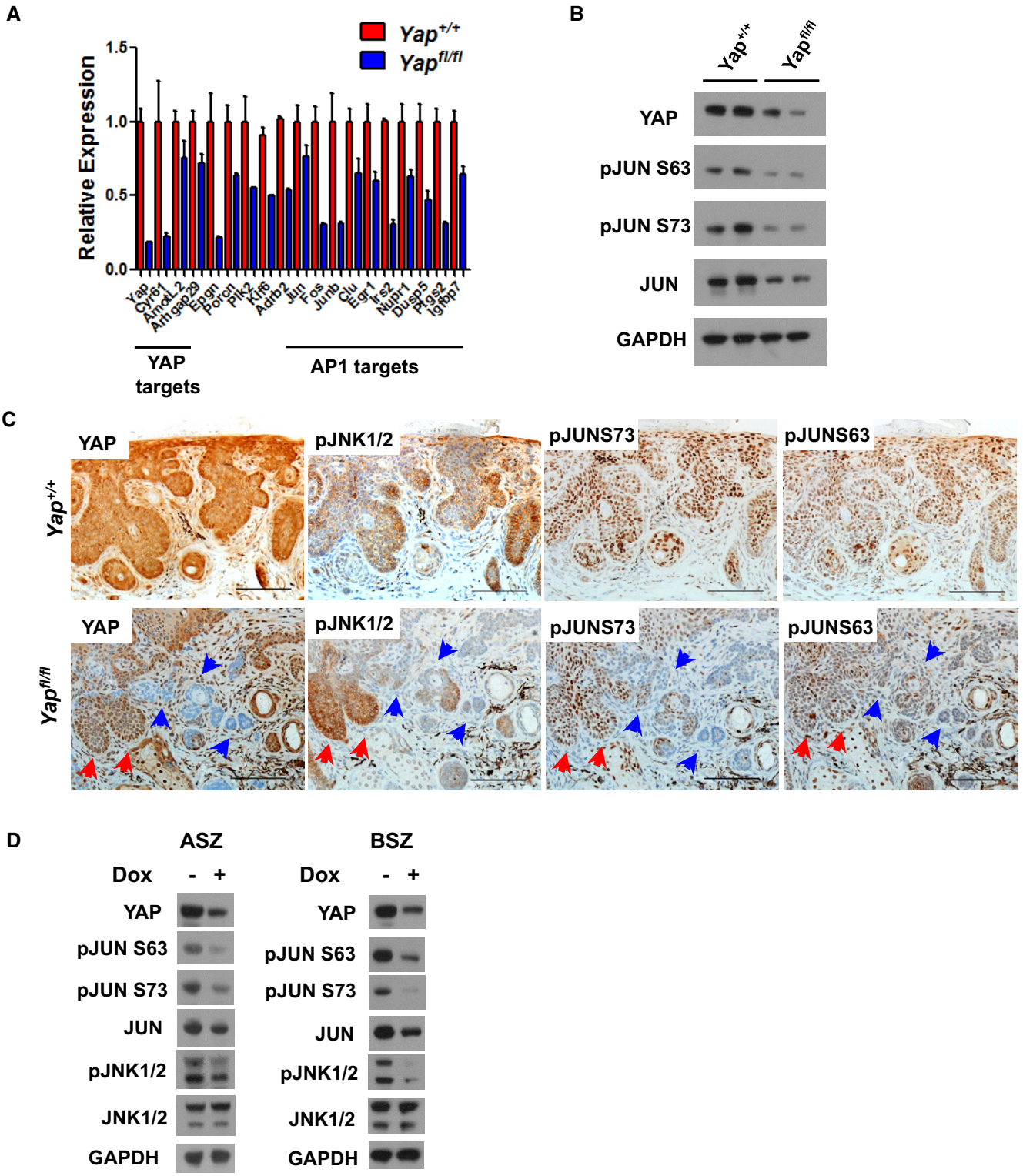

Figure 6. YAP regulates JNK-JUN activity in BCC.

A qPCR validation of differentially expressed genes indicating that YAP affects AP1 (c-JUN) target genes. Error bars represent SEM. Total of three biological replicates were used per genotype.

B Western blot analysis of JUN activity in $Yap^{+/+}$ versus $Yap^{fl/fl}$ BCC at 9 weeks after high-dose tamoxifen administration.

C IHC analysis of YAP and JNK-JUN pathway activity in $Yap^{fl/fl}$ and $Yap^{+/+}$ BCC serial sections. Red arrows indicate YAP-positive clones; blue arrows indicate YAP-negative clones. Scale bar is 100 μm.

D Western blot analysis of the JNK-JUN activity in doxycycline (Dox)-inducible *Yap* knockout (TetON-CRISPR-YapKO) in ASZ and BSZ cells.

(Harvey *et al*, 2013). Aside from cancer in adult tissues, YAP activity is critically required during emergency progenitor cell expansion for tissue repair following damage. This phenomenon has been observed in several epithelial tissues, such as skin, liver, intestine, heart, kidney, and pancreas (Patel *et al*, 2017). We speculated that skin epithelium might also exemplify a tissue where Hippo effectors, YAP and TAZ, are coerced by precise upstream cues to promote epithelial growth. Using the Hedgehog-driven BCC as a model, we show that tumors, specifically those cells located basally within a growing clone, activate YAP's transcriptional role. Though TAZ has been speculated to carry overlapping cellular functions with YAP and might compensate in a YAP-negative condition, we show that TAZ is meekly expressed in epidermis and its genetic deletion does not offer further change in BCC phenotype. However, YAP interaction with the DNA-binding transcription factors, TEAD, and co-activator function was required for BCC development. By inhibiting YAP expression in a different model where the tumor is already established, we also observe impaired BCC growth and depletion of *Yap*-null tumor cells. Detailed longitudinal analyses of the *Yap*-null BCC clones provided robust evidence that YAP is required not only for dysplastic BCC clone initiation and proliferation but also tumor survival until the invasive phenotype. Our data, however, do not distinguish whether *Yap* loss inhibits conversion of dysplastic clones to invasive tumors or whether YAP is required for the overall long-term tumor survival regardless of its progression stage. Remarkably, YAP was completely dispensable for the normal adult epidermal homeostasis. These observations support the concept that conditions such as BCC, which resemble some aspects of tissue regeneration, engage YAP activity for epithelial cell growth and thus might offer a favorable therapeutic index for targeting this pathway in cancer.

The Hedgehog–Hippo interaction and how they influence each other have been studied in several tissues and contexts (Fernandez *et al*, 2009). Based on the published reports, we speculated that YAP might be directly affecting Hedgehog signaling output and the subsequent BCC phenotype. However, we saw no change in the expression of known Hedgehog target genes (Ptch1, Gli1, Gli2, or Hhip) in *Yap*-null BCC as assessed by *in situ* hybridization or RNAseq analyses. Aside from the driver pathway, Hedgehog, Wnt signaling is the other well-established cooperating pathway significantly contributing to BCC phenotype (Yang *et al*, 2008; Youssef *et al*, 2012). Likewise, Wnt and Hippo signaling components have been shown to engage each other in numerous circumstances. Once more, we demonstrated that Wnt signaling and its EHF phenotype are absolutely unaffected in the *Yap*-null BCC. Our data show that activated YAP, independent of Hedgehog and Wnt signaling, plays a unique and vital role in driving BCC progression. Furthermore, our *in vivo* functional data explain elevated selective pressure to inactivate the Hippo regulators, *LATS1/2* and *PTPN14*, in human BCC (Bonilla *et al*, 2016).

Using unbiased RNAseq and ChIPseq analyses to decipher the mechanisms by which YAP drives BCC development and progression, we found the strongest effect on the activity of AP1 transcription complex in *Yap*-null BCC. The AP1 complex is composed of c-JUN, FOS, ATF, and MAF family homo- and heterodimers giving them highly diverse function in tissue homeostasis (Lopez-Bergami *et al*, 2010). In particular, c-JUN and FOS activity is required for the transformation and growth of tumors including those originating in skin epidermis (Lopez-Bergami *et al*, 2010). JUN depletion in BCC cells blocks their growth *in vitro* and *in vivo* (Eberl *et al*, 2012). Interestingly, YAP-TEAD-AP1 cooperation by directly interacting on the target gene promoters to regulate their expression has already been described (Zanconato *et al*, 2015; Liu *et al*, 2016). While our ChIPseq data also confirm that YAP-TEAD and AP1 could bind in close proximity at the same target genes, we find that YAP regulates overall c-JUN protein, mRNA, and transcriptional activity. The *Yap*-null BCC had significant reduction in the c-JUN phosphorylation on serines 63 and 73, two JNK phosphorylation sites that stabilize c-JUN and increase its activity. JNK inhibition in BCC cell lines reduces c-JUN phosphorylation and cell proliferation. Correspondingly, JNK activity was also diminished or increased in the tumors lacking YAP expression or YAP-overexpressing IFE lesions, respectively. Recently published findings also propose that YAP could increase JNK activity in endothelial cells (Wang *et al*, 2016). Hence, our *in vivo* and *in vitro* analyses of the JNK-JUN pathway strongly support that YAP regulates their activity in BCC. While the *Yap*-null BCC tumors or BCC cell lines show consistent reduction in phospho-JUN concomitant with decreased total c-JUN protein, we also detect decrease in c-Jun mRNA expression. Our ChIPseq data show that *c-Jun* promoter/enhancer contains TEAD binding sites but also multiple *AP1* consensus sites, which can be bound by c-JUN protein to positively regulate its own expression (Angel *et al*, 1988). In fact, c-JUN expression strongly correlated with the canonical YAP targets in various human cancer cell lines (CCLE). Thus, it is highly probable that *Yap* loss in BCC decreases YAP-TEAD transcriptional activation of the *c-Jun* promoter, JNK-mediated c-JUN phosphorylation, c-JUN protein stability, and subsequent AP1 activity. Although here we demonstrate that YAP activity potentiates the AP1 signaling in BCC, upstream molecular mechanisms linking YAP and JNK-JUN remain to be elucidated. Our RNAseq data suggest that YAP could impact MAPK signaling via transcriptional regulation of known upstream components (i.e., IRS2, IGFBP7, IGFPB2, EPGN, and DUSP5) and thus regulating JNK-JUN activity. Others have recently shown that YAP could regulate actin cytoskeleton via RHO-ROCK cascade, which also has been shown to directly control JNK-JUN axis (Marinissen *et al*, 2004; Qiao *et al*, 2017). Hereafter, future work should explore how and under which circumstances YAP impacts MAPK signaling, cytoskeleton, and JNK-JUN pathway in cancer.

In the clinic, the biggest challenge for BCC remains treatment of patients with advanced or metastatic disease, of which only about 50% respond to vismodegib therapy (Puig & Berrocal, 2015; Danhof *et al*, 2018). The mechanisms of resistance vary from emergence of the *SMO*-mutant BCC clones and activation of kinase pathways to amplification of the GLI signaling via other mechanisms (Atwood *et al*, 2013, 2015; Sharpe *et al*, 2015). As our work demonstrates that YAP drives BCC growth in a Hedgehog-independent fashion, we propose that a combination therapy of vismodegib and YAP inhibition could offer a new strategy to circumvent resistance while effectively killing BCC tumors. Furthermore, published work from our laboratory has demonstrated that sustained YAP overexpression in skin epidermis initially induces BCC-like clonal growth which eventually evolves into SCC phenotype (Schlegelmilch *et al*, 2011; Silvis *et al*, 2011). Hence, it is possible that YAP/Hippo pathway actively participates in therapy-induced BCC to SCC transdifferentiation observed in some patients. Future research should focus on

developing transdifferentiation models for better understanding YAP's contribution in this phenotype.

Materials and Methods

Animals and tumor induction

The *Yap*$^{fl/fl}$,*Yap*^{S79A,} and *Col1*$^{TetO\text{-}YAPS127A}$ mice were previously described (Schlegelmilch *et al*, 2011). The *Taz*$^{fl/fl}$ (*Wwtr1* $^{fl/fl}$) mice were previously described in Xin, M., *et al* (Xin *et al*, 2013). The *K14CreER, K14Cre*, *R26*$^{LSL\text{-}SmoM2YFP}$, *R26*$^{LSL\text{-}tdTomato}$, *TetO-Cre*, *CAG-rtTA3*, and athymic nude (*nu/nu*) mice were obtained from The Jackson Laboratories. Embryonic *Yap*-knockout skin tissue (*Yap*$^{fl/fl}$: *K14Cre*) was collected at E18.5 for analyses. The adult *Yap*-knockout (*Yap*$^{fl/fl}$ *TetO-Cre CAG-rtTA3*) or YAP^{S27A} (*Col1*$^{TetO\text{-}YAPS127A}$ *R26*$^{LSL\text{-}rtTA/+}$ *K14Cre*) overexpression was initiated at P56 (8 weeks of age) by administering doxycycline (1 g/l) with 5 g/l sucrose in drinking water for one 1 week. The *Yap*-knockout mice were followed up to 12 weeks. BCC was induced in all mice at postnatal days P24–P28 with intraperitoneal (i.p.) and/or topical tamoxifen administration. The clonal BCC induction ("low-dose" tamoxifen) was done with i.p. injections of 2.5 mg tamoxifen in 100 μl of corn oil for two consecutive days. The "high-dose" tamoxifen protocol included i.p. injections as described for the "low-dose" protocol plus simultaneous topical tamoxifen (2% tamoxifen in acetone) application on the ear and tail skin for 2 days. The ear and tail skin samples were analyzed at indicated time points following the last tamoxifen dose. To measure cell proliferation *in vivo*, mice were injected i.p. with 50 μg EdU (5-ethynyl-2′-deoxyuridine) in saline 24 h prior to euthanasia. For the allograft experiments, 5×10^6 ASZ (TetON-CRISPR-YapKO) cells in 100 μl of Geltrex® (Thermo Fisher Scientific) were injected subcutaneously into flanks of 8-week-old athymic *nu/nu* mice. The tumors were allowed to engraft for 2 weeks, after which a cohort of mice received doxycycline (1 g/l) with 5 g/l sucrose in drinking water for the duration of the experiment. All of the experiments with mice were approved by IACUC at Boston Children's Hospital.

Antibodies

Following commercially available antibodies were used: YAP (D8H1X—Cell Signaling), YAP (1A12—Cell Signaling), YAP/TAZ (D24E4—Cell Signaling), GAPDH (D16H11—Cell Signaling), pJUNS73 (D47G9—Cell Signaling), pJUNS63 (54B3—Cell Signaling), pJNK Thr183/Tyr185 (81E11—Cell Signaling), JNK (sc7345—Santa Cruz), JUN (BD 610327), GFP (ab6673—Abcam) H3K27Ac (ab4729—Abcam), TEAD1 (BD 610922), TEAD4 (ab58310—Abcam), SOX9 (AB5535—Millipore), LHX2 (sc19344—Santa Cruz), PCDH (MAB761-500 R&D Systems), LEF1 (C12A5—Cell Signaling), and CUX1 (sc13024—Santa Cruz).

Cell culture

The mouse BCC cell lines, ASZ and BSZ, were a kind gift from Ervin H. Epstein, Jr. (Children's Hospital Oakland Research Institute). The cells were grown in M154CF (Thermo Fisher Scientific) media supplemented with 0.05 mM $CaCl_2$, penicillin–streptomycin, and 10 ml chelexed FBS. The Silencer Select (Thermo Fisher Scientific) siControl (AM4611), siYap (s76160), and siTaz (s97145) RNAi were transfected into cells using Lipofectamine® RNAiMAX (Invitrogen) according to the manufacturer's protocol. The cell proliferation was measured using the CellTiter 96® AQueous One Solution Cell Proliferation Assay from Promega. JNK1/2/3 were inhibited *in vitro* with 5 μM SP600125 or DMSO, and proliferation was determined by cell counting. Doxycycline-inducible *Yap* knockout (TetON-CRISPR-YapKO) in ASZ or BSZ cells was achieved by lentiviral infection of plasmids carrying Yap sgRNA (FgH1UTG) and SpCas9 (lentiCRISPRv1; Sanjana *et al*, 2014; Aubrey *et al*, 2015). The infected cells were selected with 2 μg/ml puromycin (lentiCRISPRv1 selection) for 4 days and FACS-sorted for GFP (FgH1UTG selection). *Yap* knockout *in vitro* was induced with 1 μg/ml doxycycline treatment in culture media for 6 days. The targeting sgRNA sequence (5′-ACAACGATCAG ACAACAACA) used in our studies was directed against mouse *Yap* Exon 2.

Protein and RNA analyses

Total protein from cell lines was isolated with the ice-cold RIPA buffer containing cOmplete™ protease and PhosSTOP™ phosphatase inhibitor cocktails (Roche Applied Science). The protein concentrations were quantified with Pierce™ BCA Protein Assay Kit, and equal protein amounts were resolved on NuPAGE® Novex® 4–12% Bis-Tris protein gels (Invitrogen). Total RNA from the cell lines was isolated using TRIzol® (Invitrogen) according to the manufacturer's protocol. The RNA was converted to cDNA using iScript® (Bio-Rad) cDNA synthesis kit for qPCR analyses with either Fast SYBR Green or Fast Advanced TaqMan Master Mixes (Applied Biosystems). The qPCR primer sequences used in this study are listed in Table EV4.

Histology, Immunohistochemistry, Immunofluorescence, and RNAscope

The isolated tissues were fixed in 10% neutral buffered formalin for at least 24 h, paraffin-embedded, and sectioned onto slides to 5 μm thickness. Antigens were retrieved using Antigen Unmasking Solution (citric acid based) (Vector Labs) at 95°C for 1 h. All of the primary antibody incubations were done overnight at 4°C. For Immunohistochemistry, target protein was detected with secondary biotinylated Anti-Rabbit or Anti-Goat IgG antibodies (Vector Labs) followed by signal amplification with RTU Vectastain Elite ABC (Vector Labs). The slides were developed with DAB Peroxidase (HRP) Substrate Kit (Vector Labs), dehydrated, and mounted with Vectamount (Vector Labs). For Immunofluorescence (IF), secondary Donkey anti-Rabbit, anti-Goat, anti-Rat, or anti-Mouse Alexa Fluor®-conjugated antibodies (Thermo Fisher Scientific) were used to detect primary antibodies. Tissue-incorporated EdU was detected using the Click-iT™ Plus EdU Alexa Fluor™ 647 Imaging Kit (Thermo Fisher Scientific). All of the IF slides were mounted with Prolong Gold anti-fade with DAPI (Invitrogen) and imaged on Zeiss Axio Observer Z1 microscope equipped with Zeiss Apotome.2. The RNAscope® for Yap, Taz, Gli1, Ptch1, Axin2, and Lgr5 was done using the ACD inventoried probes and RNAscope® 2.5 HD Reagent Kit-BROWN (ACD) detection system according to the

manufacturer's instructions. De-identified human BCC tissue microarray was purchased from US Biomax, Inc.

BCC cell isolation and FACS

The RNAseq and qPCR analyses were performed on FACS-sorted ear BCC cells 6 weeks after high-dose tamoxifen administration. For the purpose of FACS sorting, we crossed *R26*$^{LSL\text{-}SmoM2YFP}$*:K14CreER* mice with *R26*$^{LSL\text{-}tdTomato}$ to use tdTomato expression as a marker for Cre recombined epidermal cells. Briefly, ear tissue from mice was minced and incubated at 37°C in 0.25% trypsin-EDTA solution for 1 h. The tissue was then passed 5–6 times through 16- and 18-gauge needle, trypsin was quenched with excess PBS containing 2% chelexed FBS, and entire solution was passed through a 70-μm filter. The cells were pelleted by centrifugation at 200 g for 15 min (4°C), washed once with PBS containing 2% chelexed FBS, and re-pelleted as before. Next, single cells were stained with indicated FACS antibodies (TER119-eFluor450, CD45-eFluor450, α6-integrin-APC) (eBiosciences) on ice for 30 min. BCC cells were FACS-sorted based on their negativity for blood markers (CD45, TER119) and positivity for tdTomato and α6-integrin. ChIPseq analysis was performed on the tail BCC 10 weeks after tamoxifen induction. First, dermal fat was scraped from the tail skin and the skin tissue was floated dermis side down onto 0.25% trypsin-EDTA solution for 1 h at 37°C. The epidermal cells were then separated from the dermis by scraping and subjected to series of filtration and centrifugation steps as described for the ear BCC.

RNAseq and ChIPseq

The RNA from the FACS sorted ear BCC cells was isolated using the RNeasy® Plus Mini Kit (Qiagen). The libraries for the RNAseq analysis were prepared using the TruSeq RNA Library Preparation Kit v2 (Illumina) according to the manufacturer's protocol. The sample preparation and chromatin immunoprecipitations with Tead1, Tead4, and H3K27Ac antibodies for the ChIPseq analyses were done as described previously (Galli *et al*, 2015). The input DNA was used as a background for defining significant signal enrichment. The ChIPseq libraries were prepared with the NEBNext® Ultra DNA Library Prep Kit and NEBNext® Multiplex Oligos for Illumina (NEB) according to the manufacturer's recommendations. All of the libraries were sequenced on the NextSeq High 75 cycles (Illumina) sequencer at Harvard University Bauer Core Facility. Differential gene expression analysis was generated using the DESeq2 package (Bioconductor) with set thresholds to adjusted P-value < 0.05 and fold change <1.5. Ingenuity Pathway Analysis (Qiagen) was done on the identified differentially expressed genes. The ChIPseq bioinformatics analysis was done as described previously (Galli *et al*, 2015). JUN or FOS co-expression correlation with other genes in human cancer cell lines was done using the Gene Neighbors tool from the Broad-Novartis Cancer Cell Line Encyclopedia (https://portals.broadinstitute.org/ccle_legacy/home).

Data accessibility

All of the RNAseq and ChIPseq data were deposited in the Gene Expression Omnibus under the accession number GSE115223.

Statistical analyses

All of the statistical tests and calculations were performed using GraphPad Prism software. Specific and appropriate statistical tests performed are indicated in the figure legends.

Expanded View for this article is available online.

Acknowledgments
We are extremely grateful to Dr. Ervin H. Epstain Jr. (CHORI) for providing us with the mouse BCC cell lines. We thank Dr. Eric Olson (UT Southwestern) for kindly providing us with *Taz*$^{fl/fl}$ mice. We also thank all the valuable scientific and technical feedback from the current and previous Camargo laboratory members. Dejan Maglic has been supported by the NRSA Postdoctoral Fellowship from NCI (5F32CA192815-03). This project was supported by the NIH/NIAMS awarded to Fernando Camargo (4R01AR064036-05). [HHS|NIH|National Institute of Arthritis and Musculoskeletal and Skin Diseases (NIAMS); HHS|NIH|National Cancer Institute (NCI)]

Author contributions
FDC, DM, and KS conceived hypotheses and generated research project plans. FDC helped write and review the manuscript. DM carried out *in vitro* and *in vivo* experiments, analyzed data, generated figures, and wrote the manuscript. KS generated preliminary data and reviewed the manuscript. AFMD helped with *in vitro* data generation and analyses. MD provided *in vivo* data and reviewed the manuscript. RP and RAC helped analyze and interpret RNAseq and ChIPseq data.

Conflict of interest
The authors declare that they have no conflict of interest.

References

Akladios B, Mendoza Reinoso V, Cain JE, Wang T, Lambie DL, Watkins DN, Beverdam A (2017) Positive regulatory interactions between YAP and Hedgehog signalling in skin homeostasis and BCC development in mouse skin *in vivo*. *PLoS One* 12: e0183178

Angel P, Hattori K, Smeal T, Karin M (1988) The jun proto-oncogene is positively autoregulated by its product, Jun/AP-1. *Cell* 55: 875 – 885

Atwood SX, Chang AL, Oro AE (2012) Hedgehog pathway inhibition and the race against tumor evolution. *J Cell Biol* 199: 193 – 197

Atwood SX, Li M, Lee A, Tang JY, Oro AE (2013) GLI activation by atypical protein kinase C iota/lambda regulates the growth of basal cell carcinomas. *Nature* 494: 484 – 488

Atwood SX, Sarin KY, Whitson RJ, Li JR, Kim G, Rezaee M, Ally MS, Kim J, Yao C, Chang ALS, Oro AE, Tang JY (2015) Smoothened variants explain the majority of drug resistance in basal cell carcinoma. *Cancer Cell* 27: 342 – 353

Aubrey BJ, Kelly GL, Kueh AJ, Brennan MS, O'Connor L, Milla L, Wilcox S, Tai L, Strasser A, Herold MJ (2015) An inducible lentiviral guide RNA platform enables the identification of tumor-essential genes and tumor-promoting mutations *in vivo*. *Cell Rep* 10: 1422 – 1432

Bonilla X, Parmentier L, King B, Bezrukov F, Kaya G, Zoete V, Seplyarskiy VB, Sharpe HJ, McKee T, Letourneau A, Ribaux PG, Popadin K, Basset-Seguin N, Ben Chaabene R, Santoni FA, Andrianova MA, Guipponi M, Garieri M, Verdan C, Grosdemange K *et al* (2016) Genomic analysis identifies new drivers and progression pathways in skin basal cell carcinoma. *Nat Genet* 48: 398 – 406

Cui X, Kim HJ, Kuiatse I, Kim H, Brown PH, Lee AV (2006) Epidermal growth factor induces insulin receptor substrate-2 in breast cancer cells via c-Jun NH(2)-terminal kinase/activator protein-1 signaling to regulate cell migration. *Cancer Res* 66: 5304 – 5313

Danhof R, Lewis K, Brown M (2018) Small molecule inhibitors of the hedgehog pathway in the treatment of basal cell carcinoma of the skin. *Am J Clin Dermatol* 19: 195 – 207

Eberl M, Klingler S, Mangelberger D, Loipetzberger A, Damhofer H, Zoidl K, Schnidar H, Hache H, Bauer HC, Solca F, Hauser-Kronberger C, Ermilov AN, Verhaegen ME, Bichakjian CK, Dlugosz AA, Nietfeld W, Sibilia M, Lehrach H, Wierling C, Aberger F (2012) Hedgehog-EGFR cooperation response genes determine the oncogenic phenotype of basal cell carcinoma and tumour-initiating pancreatic cancer cells. *EMBO Mol Med* 4: 218 – 233

Elbediwy A, Vincent-Mistiaen ZI, Spencer-Dene B, Stone RK, Boeing S, Wculek SK, Cordero J, Tan EH, Ridgway R, Brunton VG, Sahai E, Gerhardt H, Behrens A, Malanchi I, Sansom OJ, Thompson BJ (2016) Integrin signalling regulates YAP and TAZ to control skin homeostasis. *Development* 143: 1674 – 1687

Epstein EH (2008) Basal cell carcinomas: attack of the hedgehog. *Nat Rev Cancer* 8: 743 – 754

Fernandez LA, Northcott PA, Dalton J, Fraga C, Ellison D, Angers S, Taylor MD, Kenney AM (2009) YAP1 is amplified and up-regulated in hedgehog-associated medulloblastomas and mediates Sonic hedgehog-driven neural precursor proliferation. *Genes Dev* 23: 2729 – 2741

Flohil SC, Seubring I, van Rossum MM, Coebergh JW, de Vries E, Nijsten T (2013) Trends in Basal cell carcinoma incidence rates: a 37-year Dutch observational study. *J Invest Dermatol* 133: 913 – 918

Galli GG, Carrara M, Yuan WC, Valdes-Quezada C, Gurung B, Pepe-Mooney B, Zhang T, Geeven G, Gray NS, de Laat W, Calogero RA, Camargo FD (2015) YAP drives growth by controlling transcriptional pause release from dynamic enhancers. *Mol Cell* 60: 328 – 337

Goruppi S, Bonventre JV, Kyriakis JM (2002) Signaling pathways and late-onset gene induction associated with renal mesangial cell hypertrophy. *EMBO J* 21: 5427 – 5436

Harvey KF, Zhang X, Thomas DM (2013) The Hippo pathway and human cancer. *Nat Rev Cancer* 13: 246 – 257

Heintz N (2004) Gene expression nervous system atlas (GENSAT). *Nat Neurosci* 7: 483

Hoffmann E, Ashouri J, Wolter S, Doerrie A, Dittrich-Breiholz O, Schneider H, Wagner EF, Troppmair J, Mackman N, Kracht M (2008) Transcriptional regulation of EGR-1 by the interleukin-1-JNK-MKK7-c-Jun pathway. *J Biol Chem* 283: 12120 – 12128

Ito M, Yang Z, Andl T, Cui C, Kim N, Millar SE, Cotsarelis G (2007) Wnt-dependent *de novo* hair follicle regeneration in adult mouse skin after wounding. *Nature* 447: 316 – 320

Jin G, Howe PH (1997) Regulation of clusterin gene expression by transforming growth factor beta. *J Biol Chem* 272: 26620 – 26626

Johnson RL, Rothman AL, Xie J, Goodrich LV, Bare JW, Bonifas JM, Quinn AG, Myers RM, Cox DR, Epstein EH Jr, Scott MP (1996) Human homolog of patched, a candidate gene for the basal cell nevus syndrome. *Science* 272: 1668 – 1671

Larsimont JC, Youssef KK, Sanchez-Danes A, Sukumaran V, Defrance M, Delatte B, Liagre M, Baatsen P, Marine JC, Lippens S, Guerin C, Del Marmol V, Vanderwinden JM, Fuks F, Blanpain C (2015) Sox9 controls self-renewal of oncogene targeted cells and links tumor initiation and invasion. *Cell Stem Cell* 17: 60 – 73

Lee MJ, Byun MR, Furutani-Seiki M, Hong JH, Jung HS (2014) YAP and TAZ regulate skin wound healing. *J Invest Dermatol* 134: 518 – 525

Liu X, Li H, Rajurkar M, Li Q, Cotton JL, Ou J, Zhu LJ, Goel HL, Mercurio AM, Park JS, Davis RJ, Mao J (2016) Tead and AP1 coordinate transcription and motility. *Cell Rep* 14: 1169 – 1180

Lopez-Bergami P, Lau E, Ronai Z (2010) Emerging roles of ATF2 and the dynamic AP1 network in cancer. *Nat Rev Cancer* 10: 65 – 76

Marinissen MJ, Chiariello M, Tanos T, Bernard O, Narumiya S, Gutkind JS (2004) The small GTP-binding protein RhoA regulates c-Jun by a ROCK-JNK signaling axis. *Mol Cell* 14: 29 – 41

Mina M, Magi S, Jurman G, Itoh M, Kawaji H, Lassmann T, Arner E, Forrest ARR, Carninci P, Hayashizaki Y, Daub CO, the FC, Okada-Hatakeyama M, Furlanello C (2015) Promoter-level expression clustering identifies time development of transcriptional regulatory cascades initiated by ErbB receptors in breast cancer cells. *Sci Rep* 5: 11999

Nieuwenhuis E, Barnfield PC, Makino S, Hui C-C (2007) Epidermal hyperplasia and expansion of the interfollicular stem cell compartment in mutant mice with a C-terminal truncation of Patched1. *Dev Biol* 308: 547 – 560

Okamura J, Huang Y, Moon D, Brait M, Chang X, Kim MS (2012) Downregulation of insulin-like growth factor-binding protein 7 in cisplatin-resistant non-small cell lung cancer. *Cancer Biol Ther* 13: 148 – 155

Orouji A, Goerdt S, Utikal J, Leverkus M (2014) Multiple highly and moderately differentiated squamous cell carcinomas of the skin during vismodegib treatment of inoperable basal cell carcinoma. *Br J Dermatol* 171: 431 – 433

Patel SH, Camargo FD, Yimlamai D (2017) Hippo signaling in the liver regulates organ size, cell fate, and carcinogenesis. *Gastroenterology* 152: 533 – 545

Puig S, Berrocal A (2015) Management of high-risk and advanced basal cell carcinoma. *Clin Transl Oncol* 17: 497 – 503

Qiao Y, Chen J, Lim YB, Finch-Edmondson ML, Seshachalam VP, Qin L, Jiang T, Low BC, Singh H, Lim CT, Sudol M (2017) YAP regulates actin dynamics through ARHGAP29 and promotes metastasis. *Cell Rep* 19: 1495 – 1502

Ransohoff KJ, Tang JY, Sarin KY (2015) Squamous change in basal-cell carcinoma with drug resistance. *N Engl J Med* 373: 1079 – 1082

Reifenberger J, Wolter M, Knobbe CB, Kohler B, Schonicke A, Scharwachter C, Kumar K, Blaschke B, Ruzicka T, Reifenberger G (2005) Somatic mutations in the PTCH, SMOH, SUFUH and TP53 genes in sporadic basal cell carcinomas. *Br J Dermatol* 152: 43 – 51

Sanchez-Danes A, Hannezo E, Larsimont JC, Liagre M, Youssef KK, Simons BD, Blanpain C (2016) Defining the clonal dynamics leading to mouse skin tumour initiation. *Nature* 536: 298 – 303

Sanjana NE, Shalem O, Zhang F (2014) Improved vectors and genome-wide libraries for CRISPR screening. *Nat Methods* 11: 783 – 784

Schlegelmilch K, Mohseni M, Kirak O, Pruszak J, Rodriguez JR, Zhou D, Kreger BT, Vasioukhin V, Avruch J, Brummelkamp TR, Camargo FD (2011) Yap1 acts downstream of alpha-catenin to control epidermal proliferation. *Cell* 144: 782 – 795

Schnidar H, Eberl M, Klingler S, Mangelberger D, Kasper M, Hauser-Kronberger C, Regl G, Kroismayr R, Moriggl R, Sibilia M, Aberger F (2009) Epidermal growth factor receptor signaling synergizes with Hedgehog/GLI in oncogenic transformation via activation of the MEK/ERK/JUN pathway. *Cancer Res* 69: 1284 – 1292

Sharpe HJ, Pau G, Dijkgraaf GJ, Basset-Seguin N, Modrusan Z, Januario T, Tsui V, Durham AB, Dlugosz AA, Haverty PM, Bourgon R, Tang JY, Sarin KY, Dirix L, Fisher DC, Rudin CM, Sofen H, Migden MR, Yauch RL, de Sauvage FJ (2015) Genomic analysis of smoothened inhibitor resistance in basal cell carcinoma. *Cancer Cell* 27: 327 – 341

Silvis MR, Kreger BT, Lien WH, Klezovitch O, Rudakova GM, Camargo FD, Lantz DM, Seykora JT, Vasioukhin V (2011) alpha-catenin is a tumor suppressor that controls cell accumulation by regulating the localization and activity of the transcriptional coactivator Yap1. *Sci Signal* 4: ra33

So PL, Langston AW, Daniallinia N, Hebert JL, Fujimoto MA, Khaimskiy Y, Aszterbaum M, Epstein EH Jr (2006) Long-term establishment, characterization and manipulation of cell lines from mouse basal cell carcinoma tumors. *Exp Dermatol* 15: 742 – 750

Stein C, Bardet AF, Roma G, Bergling S, Clay I, Ruchti A, Agarinis C, Schmelzle T, Bouwmeester T, Schübeler D, Bauer A (2015) YAP1 exerts its transcriptional control via TEAD-mediated activation of enhancers. *PLoS Genet* 11: e1005465

Troen G, Nygaard V, Jenssen TK, Ikonomou IM, Tierens A, Matutes E, Gruszka-Westwood A, Catovsky D, Myklebost O, Lauritzsen G, Hovig E, Delabie J (2004) Constitutive expression of the AP-1 transcription factors c-jun, junD, junB, and c-fos and the marginal zone B-cell transcription factor Notch2 in splenic marginal zone lymphoma. *J Mol Diagn* 6: 297 – 307

Varelas X (2014) The Hippo pathway effectors TAZ and YAP in development, homeostasis and disease. *Development* 141: 1614 – 1626

Villani RM, Adolphe C, Palmer J, Waters MJ, Wainwright BJ (2010) Patched1 inhibits epidermal progenitor cell expansion and basal cell carcinoma formation by limiting Igfbp2 activity. *Cancer Prev Res* 3: 1222

Wang L, Luo JY, Li B, Tian XY, Chen LJ, Huang Y, Liu J, Deng D, Lau CW, Wan S, Ai D, Mak KK, Tong KK, Kwan KM, Wang N, Chiu JJ, Zhu Y, Huang Y (2016) Integrin-YAP/TAZ-JNK cascade mediates atheroprotective effect of unidirectional shear flow. *Nature* 540: 579 – 582

Wu S, Han J, Li WQ, Li T, Qureshi AA (2013) Basal-cell carcinoma incidence and associated risk factors in US women and men. *Am J Epidemiol* 178: 890 – 897

Xin M, Kim Y, Sutherland LB, Murakami M, Qi X, McAnally J, Porrello ER, Mahmoud AI, Tan W, Shelton JM, Richardson JA, Sadek HA, Bassel-Duby R, Olson EN (2013) Hippo pathway effector Yap promotes cardiac regeneration. *Proc Natl Acad Sci USA* 110: 13839 – 13844

Yang SH, Andl T, Grachtchouk V, Wang A, Liu J, Syu LJ, Ferris J, Wang TS, Glick AB, Millar SE, Dlugosz AA (2008) Pathological responses to oncogenic Hedgehog signaling in skin are dependent on canonical Wnt/beta3-catenin signaling. *Nat Genet* 40: 1130 – 1135

Youssef KK, Van Keymeulen A, Lapouge G, Beck B, Michaux C, Achouri Y, Sotiropoulou PA, Blanpain C (2010) Identification of the cell lineage at the origin of basal cell carcinoma. *Nat Cell Biol* 12: 299 – 305

Youssef KK, Lapouge G, Bouvree K, Rorive S, Brohee S, Appelstein O, Larsimont JC, Sukumaran V, Van de Sande B, Pucci D, Dekoninck S, Berthe JV, Aerts S, Salmon I, del Marmol V, Blanpain C (2012) Adult interfollicular tumour-initiating cells are reprogrammed into an embryonic hair follicle progenitor-like fate during basal cell carcinoma initiation. *Nat Cell Biol* 14: 1282 – 1294

Zanconato F, Forcato M, Battilana G, Azzolin L, Quaranta E, Bodega B, Rosato A, Bicciato S, Cordenonsi M, Piccolo S (2015) Genome-wide association between YAP/TAZ/TEAD and AP-1 at enhancers drives oncogenic growth. *Nat Cell Biol* 17: 1218 – 1227

Zhang H, Pasolli HA, Fuchs E (2011) Yes-associated protein (YAP) transcriptional coactivator functions in balancing growth and differentiation in skin. *Proc Natl Acad Sci USA* 108: 2270 – 2275

Zhao X, Ponomaryov T, Ornell KJ, Zhou P, Dabral SK, Pak E, Li W, Atwood SX, Whitson RJ, Chang ALS, Li J, Oro AE, Chan JA, Kelleher JF, Segal RA (2015) RAS/MAPK activation drives resistance to Smo inhibition, metastasis and tumor evolution in Shh pathway-dependent tumors. *Can Res* 75: 3623 – 3635